Supporting Information

A buffering PVDF-HFP-based Gel Polymer Electrolyte for Stable and Flexible Lithium Batteries

Ahmad Shokrieh[a, b, 1], *Ruichao Lu*[a, b, 1], *Binbin Zhang*[a], *Bharat Prasad Sharma*[c], *Zhixiang Wei*[a,b,*]

a. CAS Key Laboratory of Nanosystem and Hierarchical Fabrication, CAS Center for Excellence in Nanoscience, National Center for Nanoscience and Technology, Beijing 100190, P. R. China.

b. University of Chinese Academy of Sciences, Beijing 100049, P.R. China.

c. Beijing Key Laboratory of Electrochemical Process and Technology of Materials, College of Materials Science and Engineering, Beijing University of Chemical Technology, Beijing 100029, China.

Table S1. The weight percentage of DMF solvent in GPE112 during a week

Day No.	GPE112-MASS (mg)	DMF (%)
Day 1	8.82	19.64
Day 2	13.88	22.07
Day 3	8.09	21.71
Day 4	5.67	22.54
Day 7	5.83	21.91

Table S2. Mechanical properties of GPE112 and PP separator

Sample	Modulus (GPa)	Strength (MPa)	Elongation at break (%)
GPE112	7.864 ± (0.42)	110.67 ± (0.76)	41.72 ± (0.48)
PP	4.35 ± (0.12)	55.26 ± (0.34)	33.72 ± (0.77)

Table S3. Hot pressed method optimal conditions

NO.	Parameters	Magnitudes	Optimal conditions
1	Pressure (Bar)	0.5 - 1 - 1.5	0.5 bar is the best pressure and more than it makes a film supper thin and not well performance
2	Press time (s)	3 - 20 - 60	20 to 60 seconds are ok for press time
3	Temperature (°C)	100 - 150 - 180	150 °C is the best temperature. 100 °C does not stick well, 180 °C the surface structure disturbed.

Table S4. Rate and stability performance of GPE112 for different cathodes

No.	Charge and discharge condition	Sample Name	C-D voltage	Capacity loss after 100 cycles
1	**Rate test** **0.1C** **0.2C** **0.3C** **0.4C** **0.5C** **1C** **0.1C**	NCM/GPE112/Li	3-4.3V	-
2		LCO/GPE112/Li	3-4.3V	-
3		LFP/GPE112/Li	2.5-4V	-
4	**100 cycles** **0.2C**	NCM/GPE112/Li	3-4.2V	7.4%
5		LCO/GPE112/Li	3-4.2V	15%
6		LFP/GPE112/Li	2.5-4V	25.6%
7	**100 cycles** **0.5C**	NCM/GPE112/Li	3-4.2V	6.4%
8		LCO/GPE112/Li	3-4.2V	11%
9		LFP/GPE112/Li	2.5-4V	22.1%

Table S5. Mechanical properties of each component in pouch cell battery

Sample	Modulus (GPa)	Strength (MPa)	Elongation at break (%)
Copper	21.56 ± (0.68)	147.06 ± (0.56)	0.99 ± (0.71)
GPE112	7.864 ± (0.42)	110.67 ± (0.76)	41.72 ± (0.48)
Aluminum	10.13 ± (0.48)	42.94 ± (0.71)	0.63 ± (0.60)
Pouch	9.79 ± (0.37)	35.35 ± (0.43)	27.23 ± (0.52)

Table S6. The material and thickness of different layers of the pouch cell battery.

Component No.	Material	Thickness (mm)
1	Pouch	0.011
2	Copper foil	0.015
3	GPE112	0.020, 0.050 and 0.100
5	Aluminum foil	0.022

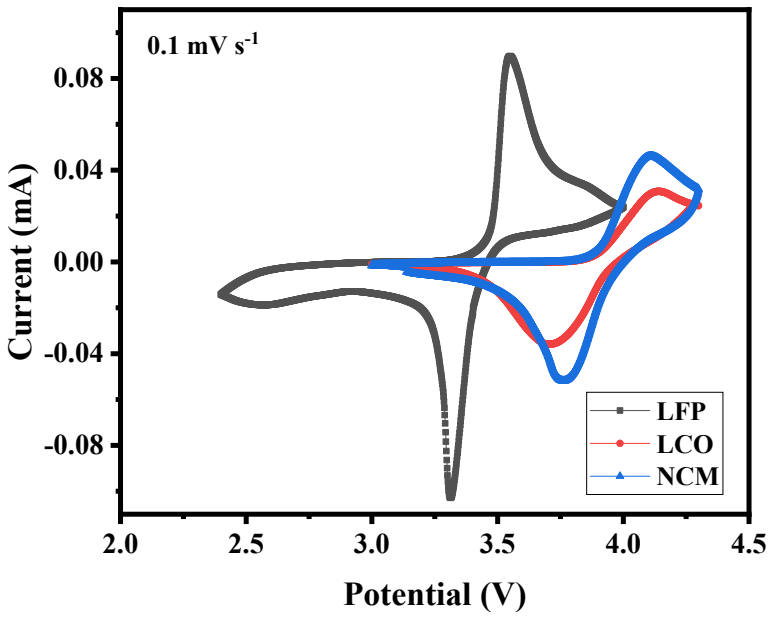

Figure S1. CV graph of LFP/Li, LCO/Li and NCM/Li full batteries with N/P ratio is around 0.034, 0.031 and 0.024 respectively, at room temperature

DFT calculation (Experimental Section)

The computational calculations for the binding of Li^+ ion with the monomer unit of PVDF-HFP Monomer, DMF molecule, and within the Li-TFSI salt have been executed using the Gaussian 16 package [1]. Geometry optimizations were performed by employing the B3LYP functional and 6-311G++(2d,p) basis set, employing tight

convergence criteria with the consideration of Grimme's van der Waal corrections [2]. The force convergence criterion was set to 10^{-6} Ha/Å, and the energy convergence criteria was set to 10^{-6} Ha. The self-consistent field (SCF) tolerance was set to qc, with a maximum of 500 SCF cycles. The frontier molecular orbitals (FMOs) calculation and the electrostatic potential (ESP) mapping of the molecules have been obtained through the single point energy calculation on the optimized molecules using the M062X functional and def2TZVP basis set. The non-bonded interactions of the lithium with the PVDF-HFP Monomer, DMF molecule, and anion of Li-TFSI salt were checked using the Multiwfn 3.8 version [3]. The binding energy for the Li^+ ion and with the PVDF-HFP Monomer, DMF molecule, and anion of Li-TFSI salt were calculated by utilizing Gibb's free energies of their optimized structures using the following equation.

$$E_{binding} = E_{total} - (E_{Li} + E_A)$$ [4]

Where, E_{total}, E_{Li}, and E_A are the energy of lithium bonded complexes, isolated Li^+ ion, and isolated A (A= PVDF-HFP Monomer, DMF molecule, or anion of Li-TFSI salt), respectively.

DFT analysis (Results and Discussions)

The optimized 3d geometries of the Li-bonded complexes have been presented in **Figure S2**. The optimum Gibbs free energies of the molecules have been observed as -5.27×10^5 kCal/mol, -160×10^5 kCal/mol, and -11.52×10^5 kCal/mol respectively for Li-PVDF-HFP, Li-DMF, and Li-TFSI complexes inferring that the salt Li-TFSI is more stable among these due to presence of ionic bond between Lithium and nitrogen. The computed binding energies **(Figure S2)** demonstrate that the interaction of Li^+ ions with the solvent DMF and the polymer matrix PVDF-HFP is feasible and spontaneous due to the presence

of electronic densities on their electronegative atoms. The lowest binding energy of the Li with TFSI anion is due to the presence of a strong ionic bond between nitrogen and lithium-ion, which is further stabilized by the presence of non-bonded interaction of lithium and oxygen. The binding energy of the Li-DMF has been observed less than Li-PVDF-HFP, suggesting the possible stabilization of Li^+ ions by DMF released from the polymer matrix PVDF-HFP during the electrochemical process [4].

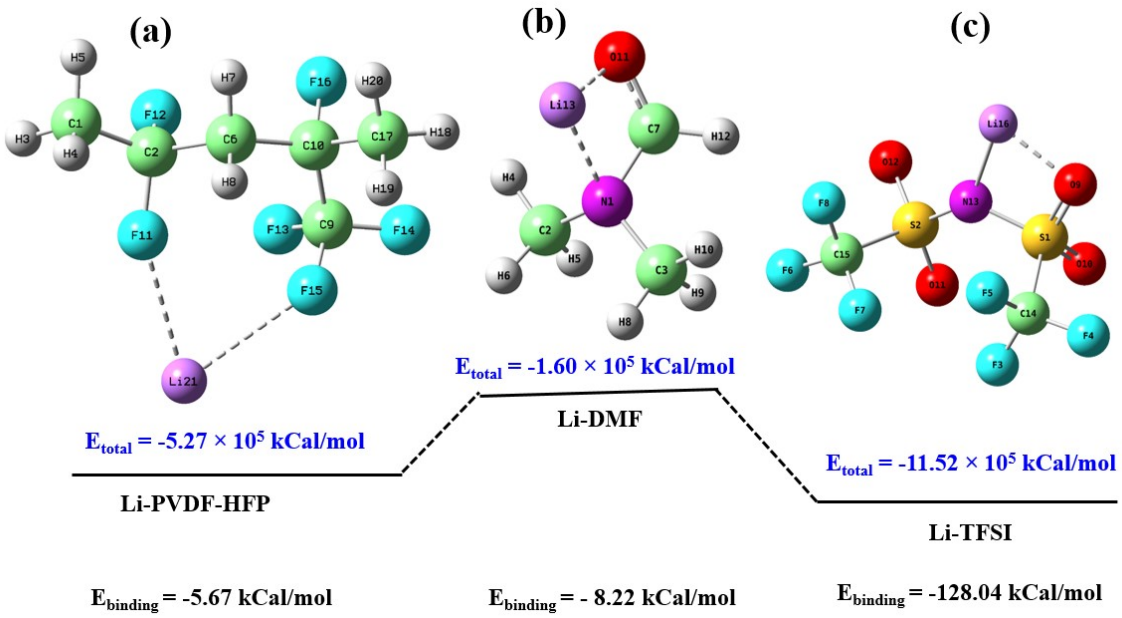

Figure S2. The optimized geometry of the (a) Li-PVDF-HFP, (b) Li-DMF, and (c) Li-TFSI with the respective binding energies.

Frontier molecular orbitals (FMOs) describe the distribution of electrons in a molecule by predicting its electronic structure and play a crucial role in understanding the interaction and reactivity of different moieties of the molecules towards nucleophilic and electrophilic centers [5]. Molecules with high-energy HOMOs can donate electrons, while molecules with low-energy LUMO can accept electrons from the electron-rich sites, thereby stabilizing the complexes. In this way, the energies of the FMOs, and the

HOMO-LUMO gap could contribute to the binding characteristics of the complex [6]. **Figure S3** depicts the computed FMOs of the lithium-bonded complexes and their respective energies. The observed lower HOMO-LUMO gap in Li-PVDF-HFP indicates its lower stability suggesting the easy removal of the lithium from the PVDF-HFP polymer during the electrochemical process. Furthermore, it has been revealed that the Li-DMF complex has more stability due to its higher HOMO-LUMO gap than the Li-PVDF-HFP complex and the stability of Li-TFSI salt has been found greater than these complex due to the presence of ionic interaction in it.

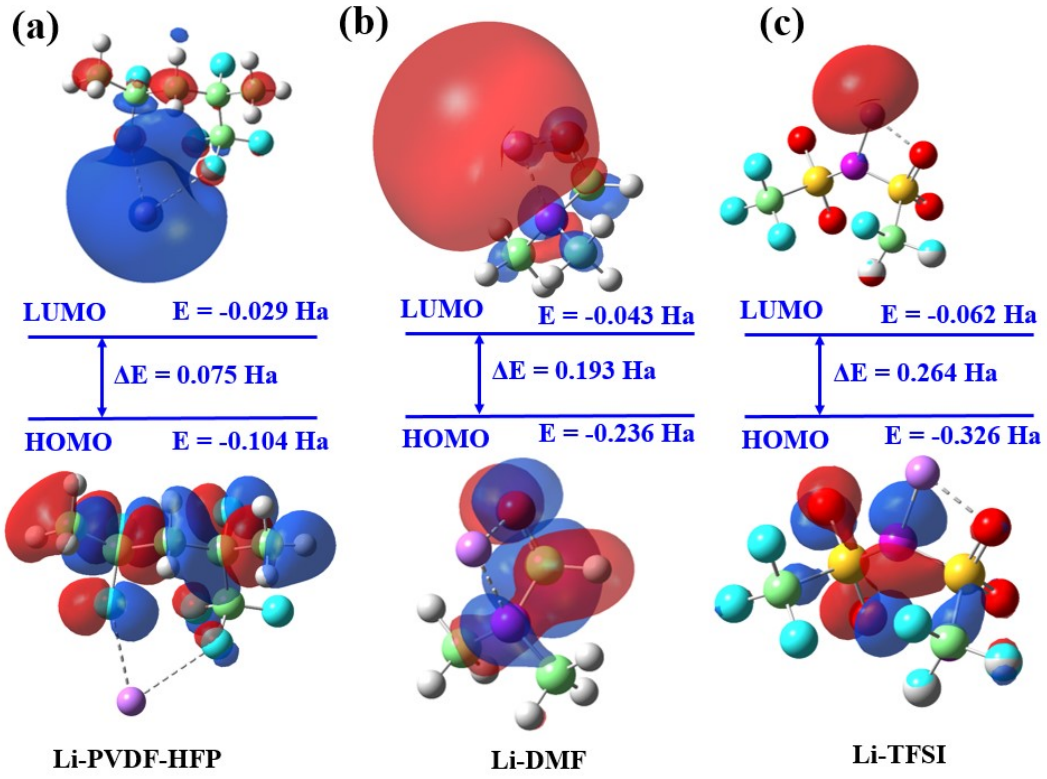

Figure S3. FMOs of (a) Li-PVDF-HFP, (b) Li-DMF, and (c) Li-TFSI (Visualized in Gauss view 6.0 with isosurface 0.03).

Furthermore, the ESP maps offer a visual representation of electron density distribution within a molecule, pinpointing regions of electron richness or deficiency. A critical analysis of ESP maps reveals the density distribution within a molecule, providing key insights into the stabilization of anomic and cationic charges [6, 7]. **Figure S4** presents the computed ESP maps of Li-PVDF-HFP, Li-DMF, and Li-TFSI. It has been found that the electron densities distributed around the fluoride atoms of polymer PVDF-HFP can effectively interact with the Li^+ ions by distributing the charges equally throughout the complex **(Figure S4-a)**. Additionally, the presence of high electron density on the oxygen of the DMF **(Figure S4-a)** facilitates its interaction with lithium by stabilizing the Li-DMF complex **(Figure S4-b)**. The electron density of the oxygen and nitrogen in the TFSI ion is not pronounced much due to the wide spreading of these groups **(Figure S4-f),** which is stabilized by the positive densities of the lithium after its binding with Li^+ ion. In this way, the ESP maps generated from the calculations highlight the significant role of DMF in stabilizing lithium ions. After the ionization of Li-TFSI salt or the detachment of lithium ions from the PVDF-HFP polymer matrix, these free lithium ions are then stabilized by DMF, as evidenced by the ESP maps. This stabilization facilitates the transport of lithium ions through the electrolyte, enhancing the overall efficiency of the ion-conducting medium.

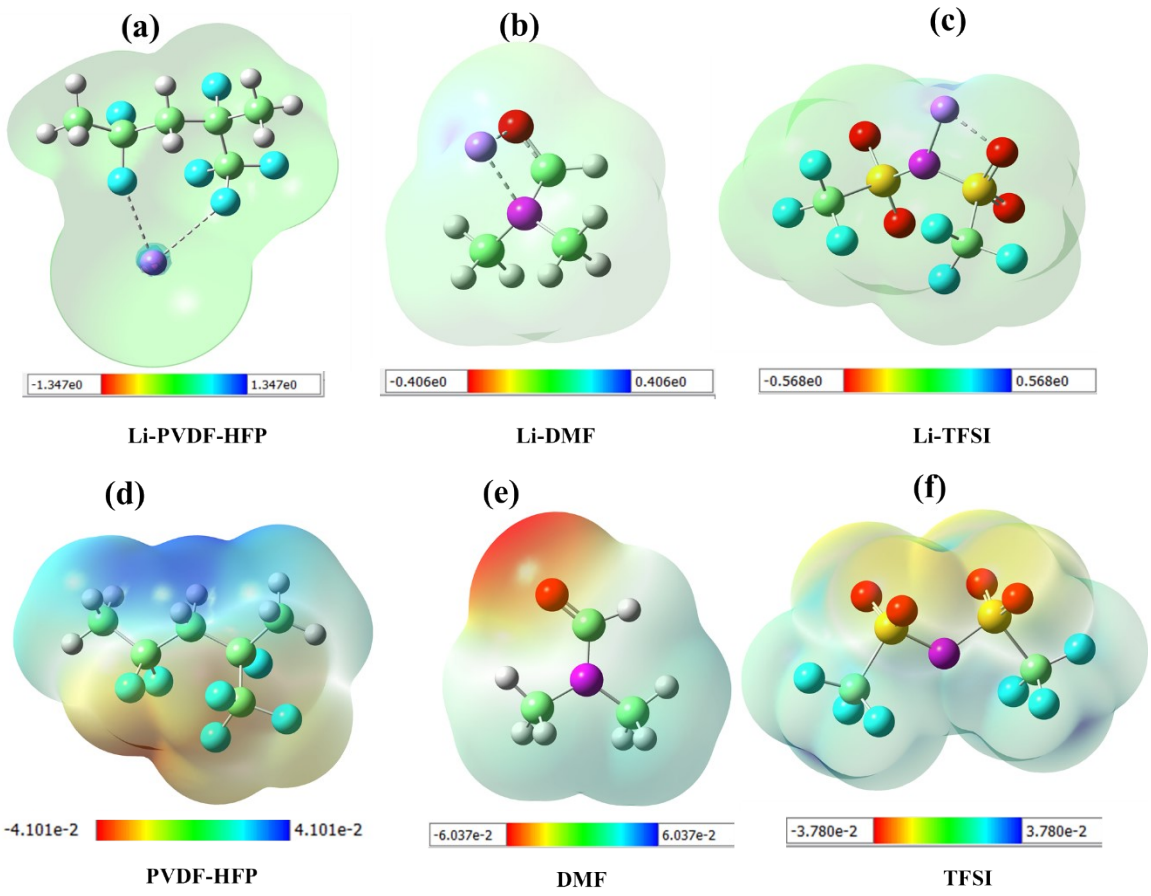

Figure S4. ESP maps of the (a) Li-PVDF-HFP, (b) Li-DMF, (c) Li-TFSI (d) PVDF-HFP, (e) DMF, and (f) TFSI (Visualized in Gauss view 6.0 with isosurface 0.0004, electron-poor regions are represented by shades of blue color, electron-rich regions, represented by shades of red color, and light yellowish parts represents the neutral region of the molecule.)

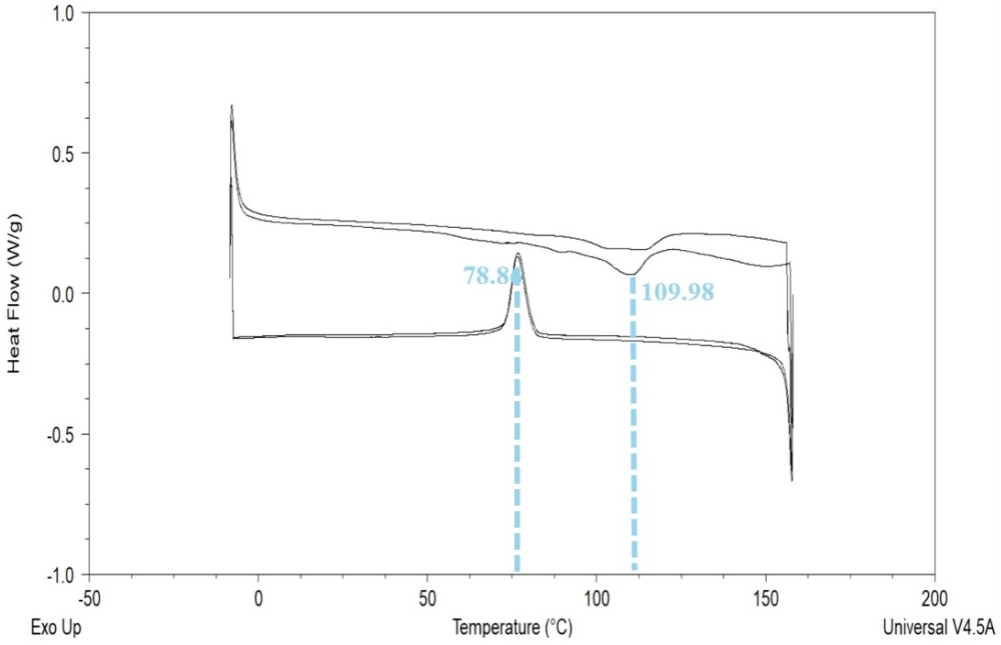

Figure S5. DSC graph of GPE112 sample in the range of 0 to 200 °C

Standard and test condition

By reviewing the standards of batteries, one may say there is no active standard or exact concept about the battery abuse tests that are accepted worldwide [8-10]. Besides, there is no clear advice on precisely specifying the mechanical loading and boundary conditions for the pouch cell [11]. **Figure S6** shows the six loading conditions for pouch cells reported in prior literature. As shown in (**Figure S6-a**), the pinch test [12-15] applies concentrated co-axial loads to the top and bottom surfaces of the pouch cell by two rigid spheres. The fixture ball radius can be changed, as it can be about several millimeters or several inches for different thicknesses of the pouch cells. As seen in (**Figure S6-b**), the hemispherical punch [16, 18] is similar to the pinch test but is easier to carry out on universal testing machines. The difference is that the battery cell is stuck on a rigid plate instead of being subjected to two symmetric loads on the two surfaces. As illustrated in

(**Figure S6-c**), out-of-plane compression loading [20-23] applies two uniform pressures to the top and bottom of the pouch cell while the side surfaces are load-free. (**Figure S6-d**) shows the in-plane compression loading test [24-27] in which two displacement boundary conditions are applied to the two sides of the pouch cell. According to the pouch cell design, the top and bottom surfaces are fully constrained by two rigid walls [27] or are subjected to a constant, consistently distributed pressure [16, 27]. (**Figure S6-e**) also illustrates the local side compression applied by a cylinder fixture [18, 19], which results in the dominant plane-strain condition in the central region due to the large width/thickness ratio of the pouch cells. (**Figure S6-f**) Depicts the 3-point bending test in which the cell is placed on two rigid supports, and the punch loading is applied at the center, thus creating a bending moment in the cell.

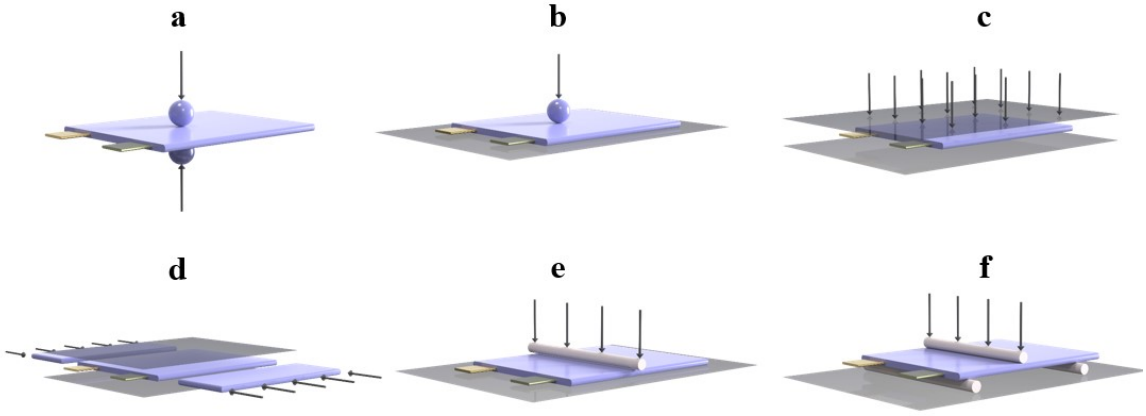

Figure S6. Several loading conditions for mechanical abuse test of pouch cell batteries: (a) pinch, (b) hemispherical punch, (c) lateral compression, (d) in-plane compression, (e) cylindrical punch, and (f) three-point bending

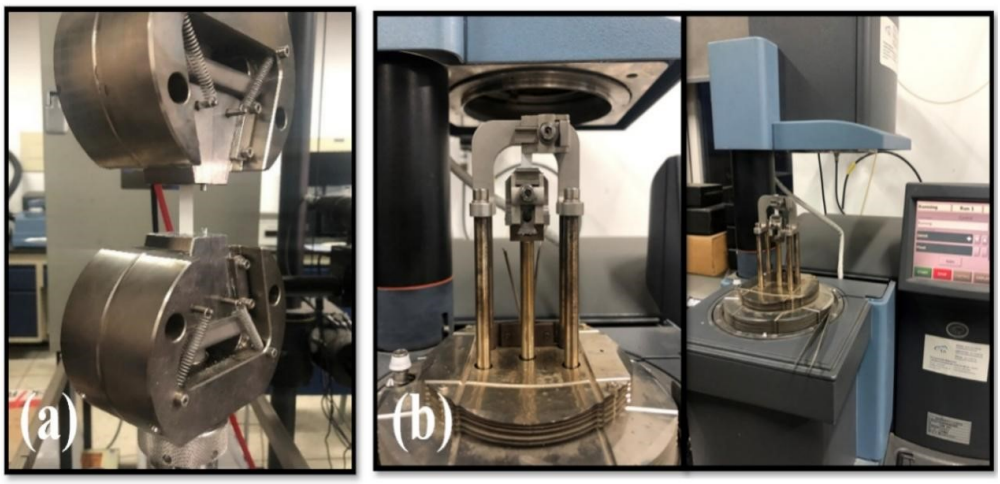

Figure S7. The GPE112 sample under the setup of (a) tensile test at 0.1 mm min $^{-1}$ (b) DMA test at 0.01 mm min^{-1}

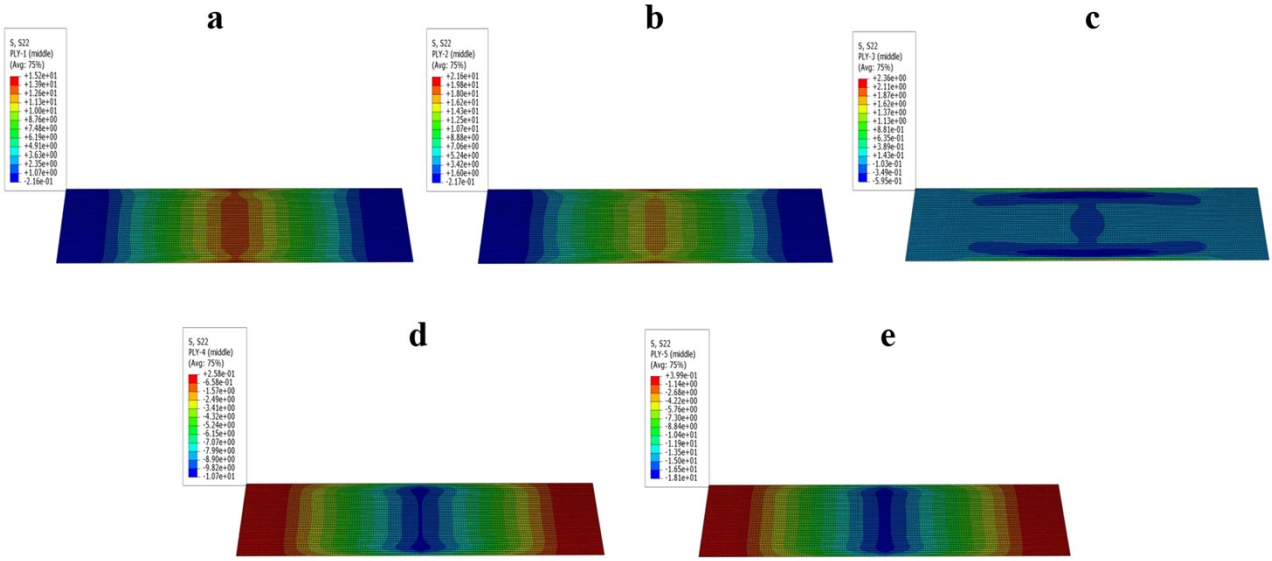

Figure S8. Contour plot of bending stress "GPE thickness = 20 µm" for (a) pouch layer, (b) Copper foil layer, (c) GPE112 layer, (d) Aluminum foil layer and (e) pouch layer

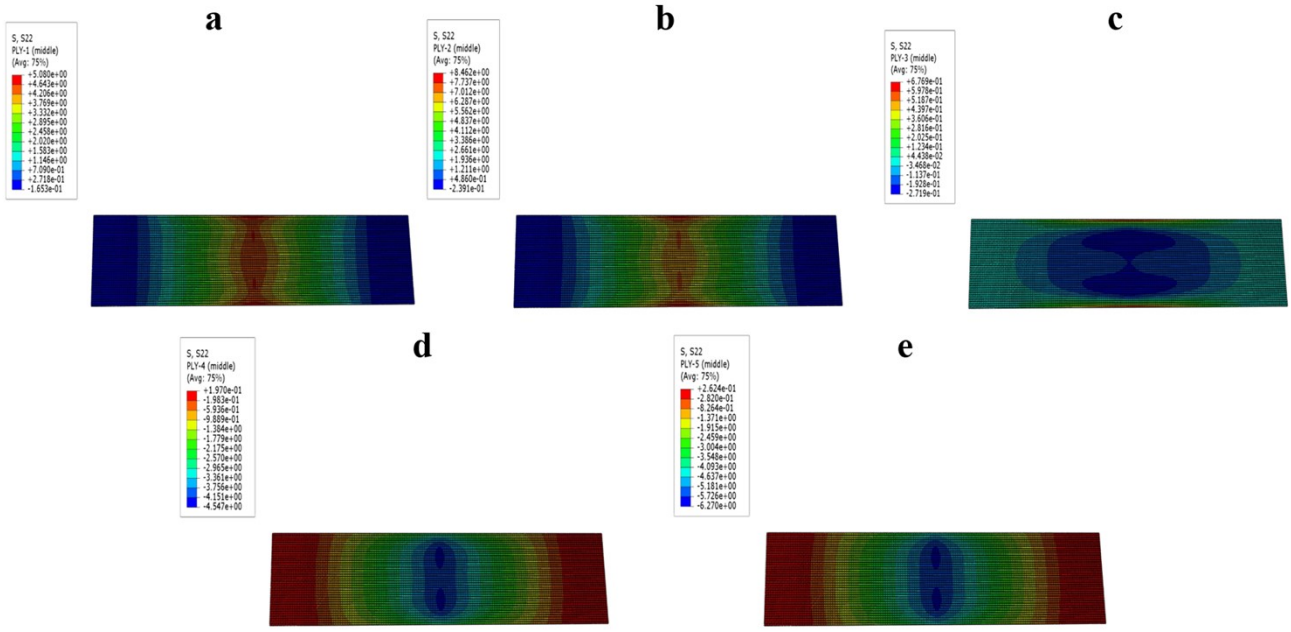

Figure S9. Contour plot of bending stress "GPE thickness = 50 µm" for (a) pouch layer, (b) Copper foil layer, (c) GPE112 layer, (d) Aluminum foil layer and (e) pouch layer

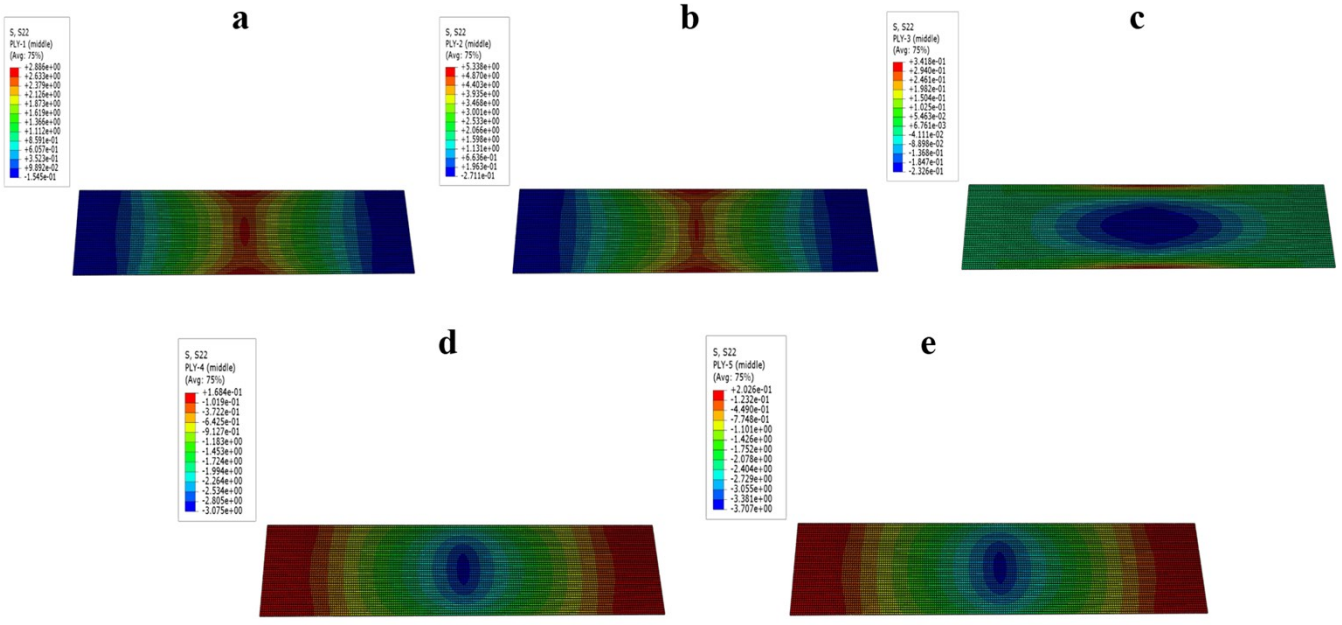

Figure S10. Contour plot of bending stress "GPE thickness = 100 μm" for (a) pouch layer, (b) Copper foil layer, (c) GPE112 layer, (d) Aluminum foil layer and (e) pouch layer

References:

[1] M. J. Frisch et al., "Gaussian 16 Rev. C.01," ed. Wallingford, CT, 2016.

[2] Sharma B.P, Adhikari Subin J, Marasini B. P, et al. "Triazole based Schiff bases and their oxovanadium(IV) complexes: Synthesis, characterization, antibacterial assay, and computational assessments [J] Heliyon, vol. 9, no. 4, p. e15239, Apr 2023.

[3] T. Lu and F. Chen, "Multiwfn: a multifunctional wavefunction analyzer," J Comput Chem, vol. 33, no. 5, pp. 580-92, Feb 15 2012.

[4] D. Guo et al., "Foldable Solid-State Batteries Enabled by Electrolyte Mediation in Covalent Organic Frameworks," Adv Mater, vol. 34, no. 23, p. e2201410, Jun 2022.

[5] B. Machura, J. G. Małecki, A. Świtlicka, I. Nawrot, and R. Kruszynski, "Copper(II) complexes of bis(pyrazol-1-yl)methane – Synthesis, spectroscopic characterization, X-ray structure and DFT calculations," Polyhedron, vol. 30, no. 5, pp. 864-872, 2011.

[6] D. Majumdar, S. Roy, J. Elizabeth Philip, B. Tüzün, and S. Hazra, "In-situ Salen-type ligand formation-driven of a heterometallic Cu(II)-Hg(II) complex: Synthetic update, crystallographic features, DFT calculations, and unveil antimicrobial profiles," Inorganic Chemistry Communications, vol. 160, 2024.

[7] B. P. Sharma et al., "Salicylaldehyde salicyloyl hydrazone and its copper(II) complex: synthesis, characterization, DFT, optical band gap, antibacterial activity, and molecular docking analysis," Journal of Coordination Chemistry, pp. 1-22, 2024.

[8] Electric and Hybrid Electric Vehicle Rechargeable Energy Storage System (RESS) Safety and Abuse Testing J2464_202108.

[9] International Organization for Standardization. Electrically propelled road vehicles - Test specification for lithium-ion traction battery packs and systems - Part 1: High-power applications, **2011**.

[10] UN/ECE Regulation No. 100.02: Uniform Provisions Concerning the Approval of Vehicles with Regard to Specific Requirements for the Electric Power Train, **2013**.

[11] Ruiz V. A review of international abuse testing standards and regulations for lithium ion batteries in electric and hybrid electric vehicles [J]. Renewable and Sustainable Energy, **2018**, *81:* 1427-1452.

[12] Wang H, Simunovic S, Maleki H, et al. Internal configuration of prismatic lithium-ion cells at the onset of mechanically induced short circuit [J]. Journal of Power Sources, **2016**, *306:* 424-430.

[13] Maleki H, Howard J. Internal short circuit in Li-ion cells [J]. Journal Power Sources **2009**, *191:* 568-574.

[14] Cai W, Wang H, Malek H, et al. Experimental simulation of internal short circuit in Li-ion and Li-ion-polymer cells [J]. Journal Power Sources, **2011**, *196:* 7779-7783.

[15] Ren F, Cox T, Wang, H. Thermal runaway risk evaluation of Li-ion cells using a pinch-torsion test [J]. Journal Power Sources, **2014**, *249:* 156-162.

[16] Sahraei E, Bosco E, Dixon B, Lai B. Microscale failure mechanisms leading to internal short circuit in Li-ion batteries under complex loading scenarios [J]. Journal of Power Sources, **2016**, *319:* 56-65.

[17] Sahraei E, Kahn M, Meier J, Tomasz W. Modelling of cracks developed in lithium ion cells under mechanical loading [J]. Royal Society of Chemistry Advances, **2015**, *5:* 80369-80380.

[18] Chung S H, Tancogne-Dejean T, Zhu J, et al. Failure in lithiumion batteries under transverse indentation loading [J]. Journal of Power Sources, **2018**, *389:* 148-159.

[19] Wang H, Watkins T R, Simunovic S, et al. Fragmentation of copper current collectors in Li-ion batteries during spherical indentation [J]. Journal of Power Sources, **2017**, *364:* 432-436.

[20] Zheng W, Lan F, Chen J, Li Z. Compression Experiment and Simulation on Prismatic Lithium-ion Batteries. DEStech Transactions on Environment Energy and Earth Science, **2018**, 393-403.

[21] Wierzbicki T, Sahraei E. Homogenized mechanical properties for the jellyroll of cylindrical Lithium-ion cells [J]. Journal of Power Sources, **2013**, *241:* 467-476.

[22] Avdeev I V, Gilaki M. Explicit Dynamic Simulation of Impact in Cylindrical Lithium Ion Batteries [J]. ASME 2012 International Mechanical Engineering Congress and Exposition, **2012**, 461-467.

[23] Xu J, Liu B, Hu D. State of Charge Dependent Mechanical Integrity Behavior of 18650 Lithium-ion Batteries. Scientific Report, **2016**, *6(21829):* 1-11.

[24] Zhu J, Zhang X, Sahraei E, Wierzbicki T. Deformation and failure mechanisms of 18650 battery cells under axial compression [J]. Journal of Power Sources, **2016**, *336:* 332-340.

[25] Ali M Y, Lai W J, Pan, J. Computational models for simulations of lithium-ion battery 231cells under constrained compression tests [J]. Journal of Power Sources, **2013**, *242:* 325-340.

[26] Mason A J. Material Characterization and Axial Loading Response of Pouch Lithium Ion Battery Cells for Crash Safety. MIT thesis, **2017**.

[27] Lai W J, Ali M Y, Pan J. Mechanical behavior of representative volume elements of lithium-ion battery cells under compressive loading conditions [J]. Journal of Power Sources, **2014**, *245:* 609- 623.